An overview of different models used in the deterministic approach for landslide susceptibility mapping

Wardatun Ahmar Abdul Manan[1*], *Mohamed* Khatif Tawaf Mohamed Yusof[2], *Siti* Marissa Abd Rahim[1], *Roslizayati* Razali[2], *Ahmad* Safuan A. Rashid[1], *Mohd* Faisal Abdul Khanan[3], and *Muhammad* Zulkarnain Abdul Rahman[3]

[1]Department of Geotechnics and Transportation, University Teknology of Malaysia, Malaysia
[2]Faculty Kejuruteraan awam University Technology of Mara, Campus Johor, Malaysia
[3]Department of Geoinformatics, University Technology of Malaysia, Malaysia

Abstract. Landslides, which can cause fatalities, property damage, and economic disruption, are some of the most catastrophic natural disasters in hilly areas. Researchers have created landslide susceptibility maps to forecast rainfall-induced landslides, particularly in hill site developments. A physically based model is more familiar in rainfall-induced landslide analysis, which consists of hydrological and infinite slope-stability models. This paper discusses the susceptibility of rainfall-induced landslides through four approaches: shallow landslide stability model, stability index mapping, transient rainfall infiltration, grid-based regional slope-stability model, and Yon-Sey slope model. The basic concepts, applications and limitations of each model are highlighted. SINMAP and SHALTAB do not consider the infiltration and groundwater flow temporally compared to TRIGRS and YS models. Nonetheless, TRIGRS solely considers 1-dimensional infiltration versus time without spatially compromising groundwater flow. Besides, YS-Slope considers regional and temporal distributions of fluctuations in groundwater variations, which can predict shallow and deep-seated failure. Further exploration needs to be carried out due to the limitations of applying these four models, which are applicable to simple landslide processes in relatively homogenous and suitable geomorphology and geology conditions.

1 Introduction

Landslides not only cause failure to slopes but also result in significant property damage and occasionally result in fatalities [1-5]. It is essential to identify landslide-prone locations to save lives and prevent severe consequences, particularly for national economies. Therefore, landslide assessments are crucial, especially in the preliminary step in the planning or design stage of the appropriate risk mitigation measures.

Global climate change causes an increase in the number of landslides due to changes in rainfall intensity, frequency and infiltration depth [6, 7]. Most researchers claim that the frequency of occurrences of intense precipitation will increase in the future, more often due to climate change [8–13]. As stated by Frattini et al. [14] and Lee et al. [15], one of the main triggering factors of landslide disasters is the concentration of heavy rainfall in a short period. At the same time, other researchers agreed that severe or excessive rainfall is a significant cause of the cataclysm [16–22].

The evaluation of rainfall-induced landslides involves the utilisation of models that assess rainfall infiltration and slope stability. This study's input data encompasses factors like topographical features, rainfall, slope material properties, and numerical techniques. These data are collected and analysed using the geometry developed and presented in the Geographic Information System (GIS). In slope stability analysis, the depth of the wetting front, which considers the initial moisture conditions, is calculated using hydrological characteristics of the soil bed, rainfall data and infiltration analysis.

In a comprehensive landslide assessment, many factors should be considered, including topography, soil properties, vegetation and precipitation [23]. The strong capability of Geographic Information Systems (GIS) in spatially distributed data processing has become popular in the last decades [24–30]. The spatial distribution of terrain parameters is crucial in assessing landslides with GIS-based analyses.

Researchers have used different landslide susceptibility techniques to compute the landslide susceptibility values. Most of them believe that landslide susceptibility maps are a great tool for planners and engineers in determining optimal locations for new development and future slope management and development planning [31–38].

The physically based approach is one of the popular methods used in the past few decades incorporating a GIS-based to assess landslide events. The physical-based approach's fundamental is structured from an infinite slope model with considerable topography, soil properties, hydrology, and ve.getation cover to comprehend and forecast landslide occurrence spatial and

* Corresponding author: wardatunahmar@graduate.utm.my

temporal patterns. This study selects SINMAP, SHALSTAB, TRIGRS and YS-slope and further discusses their application and limitations in landslide susceptibility research.

2 Theoretical models

2.1 Infinite slope stability model

The slope stability was analysed using the infinite slope failure model to calculate the factor of safety (FoS). The present model provides a comparative analysis of the resisting and driving forces acting on a plane that is parallel to the surface of a soil slope, which can be expressed in the Equation below,

$$\text{FoS}=\frac{\text{resisting component (shear strength,s)}}{\text{driving component (shear stress, }\tau\text{)}} \quad (1)$$

At the moment of failure, the gravitational force creates shear stress, τ (measured in Nm^{-2}), that is balanced by the combined strength of the soil's cohesion, c and the frictional resistance resulting from the normal stress applied on the failure plane:

$$\tau=c+(\sigma-u_a)\cdot\tan\phi \quad (2)$$

Where,

σ	Normal stress (Nm^{-2})
u_a	Pore-air pressure (Nm^{-2})
ϕ	Internal friction angle of soil (degrees)

Figure 1 shows the infinite slope in a typical slide element in saturated conditions. Based on Fredlund et al. [39], the factor of safety (FoS) can be calculated using a modified Mohr-Coulomb failure criterion as

$$FoS=\frac{c'+\sigma\tan\phi'+(u_a-u_w)\tan\phi^b}{W\sin\beta\cos\beta} \quad (3)$$

where

c'	Effective cohesion (Nm^{-2})
W	Normal stress (Nm^{-2})
u_w	Pore-water pressure (Nm^{-2})
ϕ'	Effective internal friction angle of soil (degrees)
ϕ^b	Angle due to increase in the matric suction (degrees)
β	Slope angle (degrees)

The value of ϕ^b proposed by Vanapalli et al., (1996) [40]:

$$\tan\phi^b=\tan\phi'+\frac{S-S_r}{100-S_r} \quad (4)$$

where

S_r	degree of residual saturation

While assuming that $\phi^b=\phi'$ and the pore-air pressure is at atmospheric, Equation (3) can be rewritten as

$$FoS=\frac{c'+(\sigma-u_w)\tan\phi'}{W\sin\beta\cos\beta} \quad (5)$$

Based on Equation (5), other contributing factors, such as soil properties and slope geometry, are related to the safety factor. Changes greatly influence the factor of safety in negative pore-water pressure caused by rainfall infiltration. Besides, Arairo et al. [41] have claimed that instead of changes in pore pressure variation, slope stability is also dependent on unsaturated conditions where the contribution of capillary forces to slope stability is significant. As mentioned earlier, the relationships reveal how crucial the studies in suction distribution and rainfall patterns are in association with the slope instability issue.

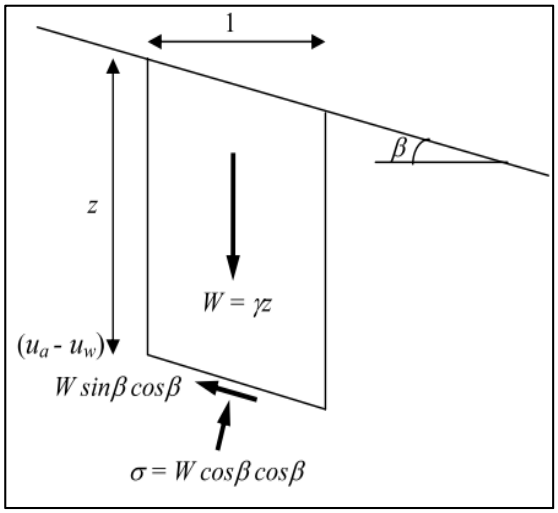

Fig. 1. Typical infinite soil element [42]

2.2 Rainfall-Induced landslides

The study of slope instability triggered by rainfall is gaining attention worldwide, particularly in countries that receive abundant rainfall throughout the year. Wang and Sassa [43] and Gerscovich et al. [44] concluded that rainfall-induced landslides happened whenever pore-water pressure and seepage force increased in soil slope leading to reduce effective stress and soil strength during periods of heavy rainfall. Xie et al. [45] study shows these failures are typically classified as shallow failures, with depths ranging from 0.5 to 2 meters. The leading cause of shallow landslides in many countries is slope saturation initiated by rainfall infiltration [46, 47]. Chen [48] has summarised that there are two types of failure mechanisms: either by continuously generating positive pore-water pressure to initiate rainfall-induced landslides or due to soil slope matric suction absorption causing shear strength reduction.

Besides, infiltration substantially influences the occurrence of landslides triggered by rainfall, as it governs the distribution of the pore-water pressure profile. The integration of Darcy's law and mass conservation principles is utilised to elucidate the process of infiltration and the distribution of pore-water pressure. Numerical simulations of infiltration effects are based on this theoretical framework. Basically, water that moves

vertically is governed by one-dimensional soil water flow in homogeneous soil. The infiltration rate, q at the soil surface is proposed using Darcy's law as

$$q=-K\left(\frac{\partial\psi}{\partial z}-1\right) \quad (6)$$

Numerous models of local infiltration such as the Horton Empirical Equation, Philip's model, and Green-Ampt Model are based on vertical homogeneous soil and various conditions to compute infiltration capacities, as shown in Equations (6– 8), respectively.

$$f_c=f_f+\left(f_0 f_f\right)exp(-\alpha t)$$

$$f_c=\frac{1}{2}St^{-1/2}+A \quad (7)$$

$$f_c=K_s\left[1-\frac{\psi_{av}(\theta_s-\theta_i)}{F}\right] \quad (8)$$

Even though many infiltration models have been developed, Morbidelli et al. [49] have discovered that calculating infiltration at various scales and slope effects is problematic due to other natural spatial heterogeneity of soil hydraulic characteristics and surface conditions.

3 Landslide susceptibility map

Landslide susceptibility mapping is the process of determining the likelihood that landslides will occur in a particular area. Various factors, including slope, elevation, slope aspect, distance to rivers and faults, and land use, are utilised to develop predictive models for identifying regions prone to landslides. These susceptibility maps have the potential to serve as important tools in the disciplines of landslide control, disaster planning, and environmental management.

The development of statistical approaches and Geographic Information System (GIS) tools for compiling landslide susceptibility or hazard maps has advanced significantly over the past decade. Recent research has shown that soft computing and data mining techniques, such as artificial neural networks and support vector machines, effectively predict landslide susceptibility. These algorithms have shown great potential in accurately identifying areas prone to landslides. In addition, physically based models consider spatial variation of soil parameters, making them more advanced and accurate for assessing slope stability. Furthermore, physically based models can incorporate temporal and spatial characteristics, allowing for a deeper comprehension of landslide susceptibility.

Overall, physically based models offer a robust and comprehensive methodology for mapping landslide susceptibility, making them essential tools for managing landslide possibility. This study aims to carry out a detailed analysis of four commonly used physically based models in landslide susceptibility research. The models under consideration are the Shallow Landslide Stability Model (SHALTAB), Stability Index Mapping (SINMAP), Transient Rainfall Infiltration and Grid-Based Regional Slope-Stability Model (TRIGRS), and Yon-Sey Slope Model (YS-Slope). This analysis will focus on the application and limitations of these models in investigating landslide susceptibility.

3.1 Stability index mapping, SINMAP

Pack et al., [50], developed the SINMAP model to enhance Colombia's existing terrain stability mapping technique. This method enhances the methodologies used for stability mapping by integrating grid-based Digital Elevation Models (DEM) into a Geographic Information System (GIS) platform using built-in free extension tools. This improvement makes the analysis more manageable, more convenient and worldwide accessible. In the present model, several parameters comprised of slope degree, slope aspect, elevation, flow direction, slope angle, and catchment area are obtained from the DEM.

On the other hand, the remaining parameters, particularly geotechnical data, must be set manually or the authors' suggested default values can be utilised. In addition, this model integrates uniform probability distributions that encompass uncertainty parameters within specified lower and higher bounds.

The stability index (SI) calculated in the SINMAP model indicates the probability of stability at a given location. This calculation assumes that the parameters are uniformly distributed within the grid cell. The value varies from zero, indicating the highest level of instability, to 1, representing the lowest level of instability. Tables 1 and 2 present a comprehensive compilation of parameters and their dimensionless SI value, organised according to stability classes.

It calculates the factor of safety in a simplified way to achieve equivalence in dry and wet density conditions according to the research conducted by Hammond et al. [51]:

$$SI=\frac{C_r+C+cos^2\theta\left[\rho_s g(D-D_w)+(\rho_s g-\rho_w g)D_w\right]tan\phi}{D\rho_s g\ sin\theta\ cos\theta} \quad (9)$$

where

C_r Root cohesion (Nm^{-2})
ρ_s Bulk density of soil (kg/m^3)
ρ_w Density of water (kg/m^3)
D Vertical soil depth (m)
D_w Height of the water table (m)

Based on the hydrological perspective, SINMAP refers to the topography-based hydrological model, TOPMODEL [50] and considered three assumptions indicated in Table 1. Assumptions (i) and (ii) in Table 1 indicate that the lateral discharge is given by $q = Ra$ and relative wetness based on the assumption (iii) can be written as

$$\bar{\omega}=min\left(\frac{Ra}{Tsin\theta},1\right) \quad (10)$$

Table 1. Assumptions in TOPMODEL [50]

(i)	The shallow lateral subsurface flow follows topographical gradients. This implies that the area contributing to the flow at any point is given by the specific catchment area a, defined by the surface topography.
(ii)	The lateral discharge q at each point has steady-state recharge R [m h^{-1}].
(iii)	The capacity for lateral flux at each point is given by $T \sin\theta$, where T is soil transmissivity [m^2 h^{-1}]; i.e., the hydraulic conductivity [m h^{-1}] multiplied by the soil thickness h [m].

The stability index can be represented by adding the wetness index from Equation (10) to the dimensionless factor of safety expressed as

$$SI = \frac{C + \cos\theta \left[1 - \min\left(\frac{Ra}{T\sin\theta}, 1\right) r\right] \tan\phi}{\sin\theta} \quad (11)$$

where

$$C = \frac{(C_r + C_s)}{(D\rho_s g)} \quad (12)$$

C is dimensionless because of the perpendicular soil thickness and $r = \rho_w/\rho_s$. The variables a and θ are derived from the DEM while C, $tan\phi$ and r values are provided by the user. The SINMAP model distinguishes between six distinct classes (**Table 2.**).

Table 2. Six stability conditions in the SINMAP model.

Condition	Class	Prediction slope Zone
SI > 1.5	1	Stable
1.5 > SI > 1.25	2	Moderate
1.25 > SI > 1.0	3	Quasy-stable
1.0 > SI > 0.5	4	Lower threshold
0.5 > SI > 0.0	5	Upper threshold
0.0 > SI	6	Defended

3.2 Shallow landslide stability model (SHALSTAB)

Montgomery and Dietrich created a physically-based shallow landslide stability model (SHALSTAB) in 1994 [48]. Assuming under steady-state conditions, the model performs distributed assessment based on the combination of infinite-slope stability analysis and a hydrological model called TOPOG [48]. This model is designed to compute the relative wetness, denoted as w, which describes the parallel flow of water along a sloping plane in steady-state saturation:

$$w = \frac{Q}{T}\frac{a}{b\ sin\beta} \quad (13)$$

where

Q Extreme rainfall that prompts landslides (mh^{-1})
T Soil's transmissivity (m^{2}h^{-1})
a Drainage area (m^2)
b Width of contour length

The SHALSTAB model can predict critical rainfall that causes slope failure in the research area by combining the hydrological and geomechanical components. The following is the main Equation to compute the essential rainfall for each grid cell.

$$log\frac{Q}{T} = \frac{\sin\beta}{a/b}\left[\frac{c}{\rho_w g z \cos^2\beta \tan\phi} + \frac{\rho_s}{\rho_w}\left(1 + \frac{\tan\beta}{\tan\phi}\right)\right], \quad (14)$$

Where

G Gravity acceleration ((m/s^2))
z Thickness of soil (m)

The predictive index value is quantified in millimeters per day of significant rainfall. The small values suggest that small intensity and short-duration rainfall may cause shallow landslides, while high rates imply that more significant rainfall is required to cause slope failure.

This model makes it possible to determine the stability of topographic elements by incorporating the geotechnical component based on the Mohr-Coulomb failure law shown in Equation (15) and Equation (13) as described in Equation (16) [52]:

$$\rho_s g z \sin\beta \cos\beta = c' + \left[\rho_s - \rho_w \frac{h}{z}\right] g z \cos^2\beta \tan\phi, \quad (15)$$

$$\frac{a}{b} = \frac{T}{Q} sin\beta \left[\frac{\rho_s}{\rho_w}\left(1 - \frac{tan\beta}{tan\phi}\right) + \frac{c'}{\rho_w g z \cos^2\beta \tan\phi}\right] \quad (16)$$

where

g Gravity acceleration ((m/s^2))
z Thickness of soil (m)

Whenever a/b exceeds the value on the right-side equation, instabilities are projected to occur whereas, the smaller value a/b indicates stable topographic elements. The reinforcement provided by roots enhances the soil's cohesive properties.

3.3 Transient Rainfall Infiltration and Grid-Based Regional Slope-Stability Model (TRIGRS)

TRIGRS uses the Fortran programming language to calculate transient changes in pore pressure and subsequent changes in the factor of safety caused by rainfall infiltration. This model generates maps of susceptibility to shallow translational landslides triggered by pluviometric events due to its output [53]. Baum et al. [54] have developed this model and updated it to version 2.0 by expanding the model to cater vertical infiltration (flow model in one-dimension) in homogenous isotropic material during a storm. The model consists of analysing one-dimensional flow through unsaturated soils and for

assessing slope stability [47]. In addition, the model acquired a GIS framework, in which the input data like elevation, slope aspect, slope inclination, soil properties, soil depth, groundwater level, and rainfall data is converted into grid-based structure, in which specific information is assigned to individual cells [21, 47].

Iverson [55] described the phenomenon of one-dimensional flow through the unsaturated soil form of Richard's equation by using coordinate transformation to consider the effect of a sloping ground surface, as mentioned in the equation below.

$$\frac{\partial\theta}{\partial t}=\frac{\partial}{\partial z}\left[K(\psi)\left(\frac{1}{cos^2\beta}\frac{\partial\psi}{\partial Z}-1\right)\right] \quad (17)$$

Where:

ψ	Pressure head of pore-water (m)
t	Time
Z	Depth (m)
θ	Volumetric water content
$K(\psi)$	Pore pressure head

The pore pressure in the Z direction depends on saturated permeability and hydraulic conductivity. This model also considers an infinite slope model to calculate the factor of safety (FS) for each cell as generally defined by Equation 17 as follows:

$$FS=\frac{tan\,\phi'}{tan\,\beta}+\frac{c'-\psi(Z,t)\gamma_w\,tan\,\phi'}{\gamma_s Z\,sin\,\beta\,cos\,\beta} \quad (18)$$

3.4 Yonsey Slope Model (YS-Slope)

Yonsey Slope Model (YS-Slope) developed by Kim et al. [23] is based on a GIS-based Physical landslide prediction model. This approach considers the progression of the wetting front through rainfall infiltration, groundwater recharge, and subsequent flow. The YS-Slope model was developed using the methodological process consisting of internal and (Fig. 2). This model consists of hydrological parameters of unsaturated soil, such as soil water characteristic curve (SWCC) and field matric suction, as well as geotechnical properties, which refer to the physical characteristics of soil that determine its strength, such as internal friction angle and cohesion value.

Three primary situations can be distinguished in describing landslides brought on by rainfall. These situations are shallow failure, which happens along the wetting front, failure at the bottom of the aquifer, and deep-seated failure which is influenced by both the wetting front and groundwater recharge.

The classification of rainfall-induced landslides encompasses three prominent conditions. They are shallow failure along the wetting front, failure at the bottom of the groundwater table, and deep-seated failure resulting from the first two conditions. To assess landslide factors triggered by rainfall, this study has utilised the infinite slope failure model, the physical limit equilibrium technique. Furthermore, the model incorporates the impact of heightened soil strength and load, as well as the interception loss caused by plants, by making modifications to the infinite slope stability equation as in the following equation:

$$FS=\frac{(c'+c_r')+\left[(\gamma_s-\gamma_w)(Z_w+D_w)+\gamma_t\cdot(D-Z_w+D_w)+q_o\right]cos^2\beta\cdot tan\phi'}{\left[\gamma_s\cdot(Z_w+D_w)+\gamma_t\cdot(D-Z_w+D_w)+q_o\right]\cdot sin\beta\cdot cos\beta} \quad (19)$$

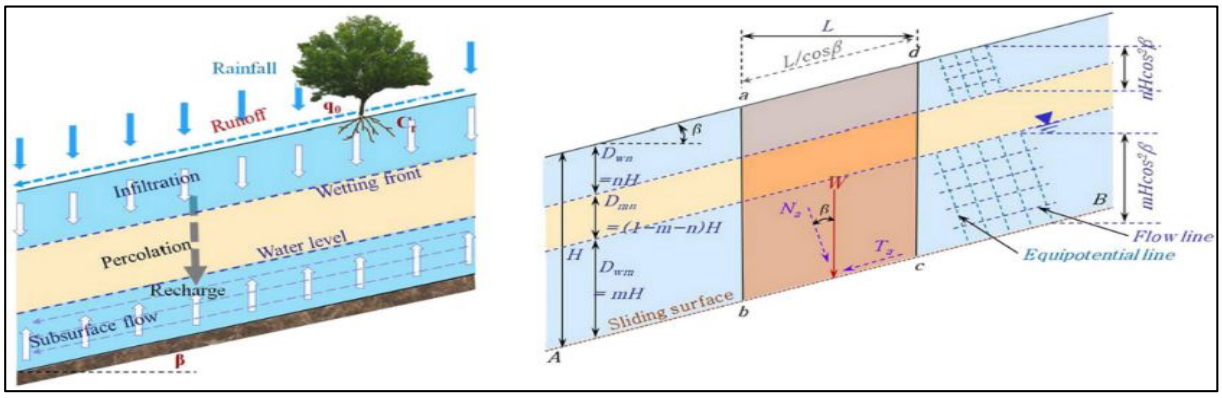

Fig. 2. Infinite slope stability analysis by Kim et al., [23].

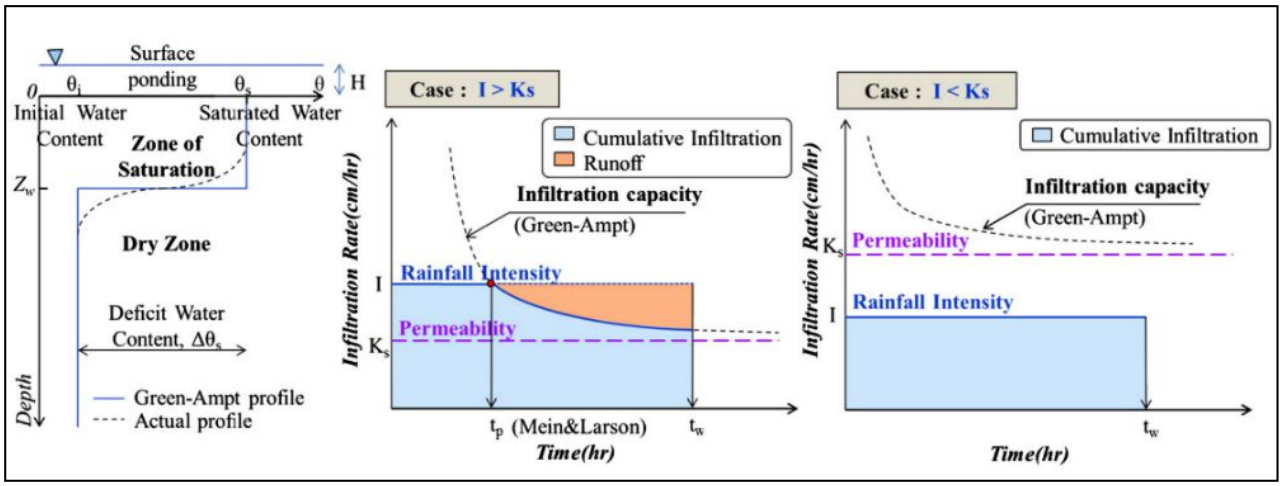

Fig. 3. Infinite slope stability analysis by Kim et al., [23].

Where,

c_r'	Shear strength by root reinforcement
q_o	Load from forest tree
γ_t	Total unit weight of soils
Z_w	Wetting front depth
D_w	Groundwater table from the bedrock
D	Thickness of dry soil

The presence of forest trees contributes to the augmentation of driving and resistance forces, whilst root reinforcement increases resistance in slope stability. Mein and Larson [50] have adopted the modified Green-Ampt model to analyse rainfall infiltration and estimate wetting front depth as follows

$$I_R = I \cdot t_p + \int_{t_p}^{t_w} K_s \left(1 + \frac{\psi_f \Delta\theta}{F}\right) \quad (20)$$

$$t_p = \frac{K_s \cdot \psi_f \cdot \Delta\theta}{I_R \cdot (K_s - I_R)} \quad (21)$$

$$D_{wn} = \frac{I_R}{\Delta\theta} = \frac{I \cdot t_p + \int_{t_p}^{t_w} K_s \left(1 + \frac{\psi_f \Delta\theta}{F}\right)}{\Delta\theta} \quad (22)$$

The equation (20) represents rainfall infiltration, I_R and is estimated using the trial and error method with a cumulative infiltration variable. The relationship between rainfall infiltration and runoff is calculated by considering the ponding time, t_p [50]. The depth of the wetting front, denoted as D_{wn}, within the vadose zone can be empirically defined as the ratio of the rainfall-infiltration, I_R and the deficit water content, $\Delta\theta$.

The trial-and-error approach was utilised to ascertain the ponding duration and cumulative infiltration by employing Equations (20) and (21) as each parameter is interdependent on these factors, it becomes important to consider all of them. Cumulative infiltration, which is subsequently utilised to compute the duration of ponding is determined by comparing the computed cumulative infiltration using Equations (21) with the cumulative infiltration assumed.

The total infiltration and the shortfall water content are used to determine the wetting front's depth. The aforementioned methodology is used for every individual grid point inside the geographical information system (GIS) geometry to ascertain the regional wetness state of the designated study area. The depth of the wetting front significantly affects slip surface strength and overburden pressure of initial debris flow simulation. Additionally, it is considered when calculating the erosion depth

Table 3: Summaries of four models

Model	SINMAP	SHALSTAB	TRIGRS	YS-SLOPE
Type of landslide	Shallow translational failure	Shallow translational failure	Shallow translational failure	Shallow and deep-seated failure
Soil condition	saturated	saturated	unsaturated	Unsaturated
Hydrological model	steady state	steady state	transient rainfall	hydrometeorological
Infiltration	Not considered	Not considered	pore pressure response	Infiltration depth
Subsurface flow condition	uniform	uniform	Not considered	Homogeneous, Varies with time and below the groundwater table.
Trigger slope stability	probability of FS	critical steady-state rainfall	Limit equilibrium slope stability model	Limit equilibrium slope stability model
Output	Stability Index (SI)	steady-state recharge	Factor of Safety (FS)	Factor of Safety (FS)

The researchers utilised a modified version of the Green and Ampt model to assess the infiltration of rainfall and subsequent recharge of groundwater, considering the characteristics of the unsaturated soil. The hydrological model is based on three assumptions: (1) assumes that both the aquifer and soils are homogeneous in nature; (2) acknowledges that recharge rates vary both geographically and temporally; (3) model assumes that groundwater flows occur only beneath the ground surface.

The calculation of groundwater flow was performed by integrating a raster model based on Geographic Information Systems (GIS) with Darcy's equation. The input variable for the calculation of recharge was the infiltration of rainfall. The Green-Ampt model, after being updated, was employed to analyse rainfall infiltration. It was recommended as a suitable model for studying infiltration in homogeneous soils with a consistent water content when subjected to ponded circumstances. The Green-Ampt model was adapted to better suit the modelling of infiltration. A groundwater flow analysis was performed on discrete units with homogeneous soil properties. The fluxes were computed to achieve equilibrium between the quantities of water entering and exiting the unit volume, by Darcy's law.

4 Result and discussion

Among these models, SHALSTAB and SINMAP have a similarity in conception framework that incorporates geotechnical, hydrological, and geomorphic input parameters. Although the constitution of these two models is similar, SHALSTAB is classified under a deterministic approach, while SINMAP is probabilistic. Besides, SHALSTAB calculates critical precipitation for slope failure, while SINMAP, TRIGS, and YS-slope determine the factor of safety. According to Bueechi et al. [57], the use of arbitrary parameters in the SINMAP model strongly restricts the model results. Hence, it is advisable to utilise the outcomes solely as a broad measure of vulnerability rather than as a factor of safety.

Pradhan and Kim [58] conducted a comparative analysis of the application of the SHALSTAB and SINMAP models for slope assessment in Deokjeok, Korea. The results of their analysis revealed that the susceptibility maps generated by the SHALSTAB model exhibited a significantly higher prediction accuracy of 82.4%. In contrast, the SINMAP model demonstrated a comparatively lower prediction accuracy of 62.58%. The researchers concluded that the SHALSTAB model exhibited more accuracy in forecasting regions susceptible to landslides in weathered granite soils. Furthermore, they observed and found that the landslides concentrated in areas identified as highly unstable.

Michel et al. [59] compared SHALSTAB and SINMAP by assessing their effectiveness in delineating areas prone to landslides throughout the Cunha River basin in Brazil. The outcomes derived from the simulation of both models demonstrated satisfactory accuracy in predicting landslides within this basin. All observed landslide scars exhibited a consistent correspondence with the unstable classes identified by the SHALSTAB and SINMAP models.

In the context of a comparison analysis, it was shown that the optimal values of SuI/ErI derived from maps constructed using the SHALSTAB and SINMAP methodologies were 3.08 and 3.11, respectively. Regarding identifying landslide scars into the unstable classes, SHALSTAB demonstrated better performance than SINMAP in reclassifying the stability map. According to the SHALSTAB classification, a mere 6% of the basin's overall area was deemed unstable, whereas SINMAP categorised a significantly higher proportion of 30%.

They concluded that the SHALSTAB model demonstrates a higher capability in identifying specific regions that are susceptible to shallow landslides compared to the SINMAP model when it comes to landslide prediction within the Cunha River basin. Besides, Kim et al., [23] mentioned in their study although both SHALSTAB and SINMAP take into consideration shallow landslide due to groundwater flow convergence and TRIGRS model depends on pore water pressure analysis, these three models cannot investigate the critical condition of groundwater flow due to rainfall infiltration that affects slope stability.

Although all four models are similar in their development, it should be noted that SINMAP and SHALTAB do not consider unsaturated circumstances compared to TRIGRS and YS slope. While the TRIGRS model only considers temporal infiltration in a one-dimensional condition, the YS slope model incorporates groundwater variation in both spatial and temporal distribution. Therefore, the YS slope model can predict failures occurring at both shallow and deep-seated levels. Table 3 presents a summary of the four models.

5 Conclusion

In conclusion, developing landslide susceptibility maps requires various techniques that have different abilities. The feasibility of conducting a study relies on the accessibility of an extensive database and the particular goals of the research. These maps are useful resources for urban planners and engineers as they work towards managing and preventing landslides from happening in the future.

This work was sponsored by the UTM Fundamental Research Grant awarded by Universiti Teknologi Malaysia (Impact of climate change on the mechanical behaviour of cement-treated lateritic soil - Q.J130000.3851.21H90) and the Ministry of Higher Education of Malaysia for the Fundamental Research Grant Scheme – FRGS/1/2022/TK06/UTM/02/14.

References

1. B. D. Collins and D. Znidarcic, J. Geotech. Geoenvironmental Eng., **130**, 362–372 (2004)
2. G. Formetta, G. Capparelli, and P. Versace, Hydrol. Earth Syst. Sci., **20**, 4585–4603 (2016)

3. S. Kawagoe, S. Kazama, and P. R. Sarukkalige, Hydrol. Earth Syst. Sci., **14**, 1047–1061 (2010)
4. C. Lepore, E. Arnone, L. V. Noto, G. Sivandran, and R. L. Bras, Hydrol. Earth Syst. Sci., **17**, 3371–3387 (2013) Arab. J. Geosci., **8**, 3183–3194 (2014)
5. N. Saadatkhah, A. Kassim, and L. M. Lee, J. Geosci., **8**, 3183–3194 (2014)
6. M. Borga, G. Dalla Fontana, and F. Cazorzi, J. Hydrol., 268, 56–71 (2002)
7. Z. Liao, Y. Hong, D. Kirschbaum, R. F. Adler, J. J. Gourley, and R. Wooten, Nat. Hazards, **58**, 325–339 (2011)
8. J. A. Coe, Geology, **40**, 323–326 (2012)
9. S. L. Gariano and F. Guzzetti, Earth-Science Rev., **162**, 227–252 (2016)
10. L. Moung-Jin, S. Won-Kyong, W. Joong-Sun, P. Inhye, and L. Saro, Geocarto Int., **29**, 639–662 (2014)
11. S. Protong, P. A. Carling, and J. Leyland, assessment in uttaradit province, Thailand, Eng. J., **22**, 243–255 (2018)
12. L. Sangelantoni, E. Gioia, and F. Marincioni, Springer Netherlands, **93**, 2 (2018)
13. K. J. Shou and C. M. Yang, Eng. Geol., **192**, 46–62, (2015)
14. P. Frattini, G. Crosta, and A. Carrara, Eng. Geol., **111**, 62–72 (2010)
15. M. J. Lee, I. Park, J. S. Won and S. Lee, Geomatics, Nat. Hazards Risk, **7**, 424–446 (2016)
16. D. Kazmi, S. Qasim, I. S. . Civ. Eng. J., **2**, no. 12, pp. 669–678 (2016)
17. J. Kim, S. Jeong, S. Park, and J. Sharma, Eng. Geol., **75**, 251–262 (2004)
18. L. Montrasio and R. Valentino, Nat. Hazards Earth Syst. Sci., **8**, 1149–1159 (2008)
19. M. Mukhlisin, S. J. Matlan, M. J. Ahlan, and M. R. Taha, J. Teknol., **72**, 15–21 (2015)
20. A. S. Muntohar and H. J. Liao, Environ. Geol., **56**, 1145–1159 (2009)
21. N. Saadatkhah, A. Kassim, L. M. Lee, and J. Rahnamarad, Environ. Earth Sci., **73**, 8425–8441 (2015)
22. M. Y. Sakamoto, L. H. Guesser, R. J. Contessi, R. A. R. Higashi, V. S. Müller, and R. M. Sbroglia, Eng. Slopes. Exp. Theory Pract., **3**, 1783–1790 (2016)
23. J. Kim, GIS-based Susceptibility Assessment of Landslides using Geotechnical and Hydrological Model, Yonsei University, (2014)
24. P. Biswajeet and L. Saro, Earth Sci. Front., **14** 143–151 (2007)
25. A. Carrara, M. Cardinali, F. Guzzetti, and P. Reichenbach, Gis Technology in Mapping Landslide Hazard, 135–175 (1995)
26. A. Carrara and R. J. Pike, GIS technology and models for assessing landslide hazard and risk, Geomorphology, **94,** 257–260 (2008)
27. N. Christanto, Hydrological – Slope Stability Modeling for Landslide Hazard Assessment by means of GIS and Remote Sensing Data, Assessment, 89, (2008)
28. D. R. Montgomery, K. Sullivan, and H. M. Hydrol. Process., **12**, 943–955 (1998)
29. S. Sarkar and D. P. Kanungo, **70**, 617–625 (2004)
30. M. Xie, T. Esaki, and M. Cai, J. Geotech. Geoenvironmental Eng., **132**, 656–660 (2006)
31. W. Chen, H. Chai, Z. Zhao, Q. Wang, and H. Hong, Environ. Earth Sci., **75**, 474 (2016)
32. M. Ercanoglu and C. Gokceoglu, Environ. Geol., **41**, 720–730 (2002)
33. B. Feizizadeh, M. S. Roodposhti, T. Blaschke, and J. Aryal, Arab. J. Geosci., **10**, 122 (2017), doi: 10.1007/s12517-017-2918-z.
34. H. R. Pourghasemi, B. Pradhan, and C. Gokceoglu, , Appl. Mech. Mater., **225**, 486–491 (2012)
35. H. R. Pourghasemi, H. R. Moradi, and S. M. Fatemi Aghda, Nat. Hazards, **69**, 749–779 (2013)
36. B. Pradhan and S. Lee, Environ. Earth Sci., **60**, 1037–1054 (2010)
37. T. H. Wu, W. H. Tang, and H. H. Einstein, Spec. Rep. - Natl. Res. Counc. Transp. Res. Board, **247**, 106–118 (1996)
38. M. and C. W. S. Zakaria, Geol. Soc. Malaysia Bull., **46**, 69–73 (2003)
39. D. G. Fredlund, N. R. Morgenstern, and R. A. Widger, Can. Geotech. J., **15**, 313–321 (1978)
40. S. K. Vanapalli, D. G. Fredlund, and D. E. Pufahl, Geotech. Test. J., **19**, 259–268 (1996)
41. W. Arairo, F. Prunier, I. Djeran-Maigre, and A. Millard, Environ. Geotech., **3**, 36–46 (2016)
42. L. M. Lee, Influence of Rainfall Pattern on Suction Distribution and Slope Stability 359 (2008)
43. G. Wang and K. Sassa, Eng. Geol., **69**, 109–125 (2003)
44. D. M. S. Gerscovich, E. A. Vargas, and T. M. P. de Campos, Eng. Geol., **88**, 23–40 (2006)
45. M. Xie, T. Esaki, and M. Cai, Environ. Geol., **46**, 840–850 (2004)
46. A. M. S. Pradhan and Y. T. Kim, CATENA, **140**, 125–139 (2016)
47. J. Zhuang, J. Peng, G. Wang, J. Iqbal, Y. Wang, W. Li, Q. Xu and X. Zhu, Earth Surf. Process. Landforms, **42**, 915–927 (2017)
48. H. Chen, Cell -Flow Risk Assessment And Early Warning 322 (2015)
49. R. Morbidelli, C. Corradini, C. Saltalippi, A. Flammini, J. Dari, and R. S. Govindaraju, (Switzerland), **10**, 12 (2018)
50. Mein and C. Larson, Res., **9**, 384–394 (1973)
51. C. Hammond, D. Hall, S. Miller, and P. Swetik, , Gen. Tech. Rep. - US Dep. Agric. For. Serv., 285 (1992)
52. E. Aristizábal, E. García, and C. Martínez, Nat. Hazards, **78**, 621–634 (2015)
53. F. de L. R. Listo, M. C. V. Gomes, and F. S. Ferreira, J. South Am. Earth Sci., (2020)
54. R. L. Baum, W. Z. Savage, and J. W. Godt. U.S. Geol. Surv. Open-File Rep., 2008–1159 (2008)
55. R. M. Iverson , Res., **36**, 1897–1910 (2000)
56. J. Kim, K. Lee, S. Jeong, and G. Kim, Eng. Geol., **182**, 63–78 (2014)
57. E. Bueechi, J. Klimeš, H. Frey, C. Huggel, T. Strozzi, and A. Cochachin, Landslides, **16**, 395–407 (2019)
58. A. M. S. Pradhan and Y. T. Kim, Environ. Earth Sci., **73**, 5761–5771 (2015)
59. G. P. Michel, M. Kobiyama, and R. F. Goerl, J. Soils Sediments, **14**, 1266–1277 (2014)